RECENT IMPROVEMENTS AND CURRENT UNCERTAINTY BUDGET OF PTB FOUNTAIN CLOCK CSF2

V. Gerginov[(1)], N. Nemitz[(1)], D. Griebsch[(1)], M. Kazda[(1)], R. Li[(2)], K. Gibble[(2)], R. Wynands[(1)] and S. Weyers[(1)]

[(1)]Physikalisch-Technische Bundesanstalt (PTB),
Bundesallee 100, 38116 Braunschweig, Germany
Email: Vladislav.Gerginov@ptb.de

[(2)]Department of Physics, The Pennsylvania State University,
University Park, Pennsylvania 16802, USA
Email: kgibble@phys.psu.edu

INTRODUCTION

The second fountain primary frequency standard CSF2 at Physikalisch-Technische Bundesanstalt (PTB) has been contributing to International Atomic Time (TAI) since December 2008 [1]. Since November 2009, the fountain has been operating with a new source of slow atoms. This Low-Velocity Intense Source (LVIS) [2] significantly improves the molasses loading rate and up to 1.5×10^{9} atoms can now be loaded in 1 s. Thus the short-term instability of the fountain is improved from 2.5×10^{-13} $(\tau/s)^{-1/2}$ to 1.7×10^{-13} $(\tau/s)^{-1/2}$. The statistical uncertainty of collisional shift evaluations is also reduced to below 2.0×10^{-16} for a 24-hour collisional shift measurement duration due to both the reduced short term instability and the larger range of cloud densities possible.

FOUNTAIN OPERATION USING THE SLOW ATOMIC BEAM SOURCE

The slow atom source was designed to launch atoms in the horizontal plane towards the molasses region. The design and performance of the LVIS will be given elsewhere [3], and here only a brief description will be presented. The LVIS setup has a typical MOT arrangement. Two lasers at 852 nm wavelength – for cooling and repumping, based on distributed feedback (DFB) technology – are sent to the setup via polarization-maintaining optical fibers. As in a MOT, the LVIS setup has two laser beam pairs of collimated counter-propagating beams with circular polarizations. A fifth collimated circularly-polarized laser beam is used in the direction along which the atoms are ejected from the LVIS. A quarter wave plate with a highly reflective coating on the back side provides the counterpropagating beam for this axis. A hole with 0.5 mm diameter in the center of the plate creates a shaded region and forms an exit aperture for the ejected atoms. Caesium atoms captured from the background gas gradually move towards the trap center until they enter the center region at a very low velocity. They are then pushed towards the waveplate due to the local imbalance in light pressure. The atoms that escape through the hole form a well collimated beam with a mean velocity of 11 m/s and an estimated flux of 1.5×10^{9} atoms/s. The beam vacuum system is designed to allow the atoms to follow a ballistic trajectory into the molasses region of the fountain.

The slow beam atom loading has several advantages over loading from a thermal atomic vapor. First, it helps improve the short-term instability of the fountain by the increased loading rate. Second, it allows for more accurate evaluation of the collisional shift uncertainty, as higher atomic densities can be reached with the faster loading. Third, it reduces the partial pressure of caesium in the molasses region of the fountain as the source of caesium is now close to the centre of the slow beam vacuum vessel. The differential pumping due to the small open area around the edges of the wave plate and a graphite getter installed behind it reduce the pressure measured below the molasses zone to 5×10^{-7} Pa.

For each fountain cycle, the lasers used in the slow atomic beam source are switched on by opening a mechanical shutter. The loading time for normal operation is 250 ms (which includes the time of flight between the loading zone of the LVIS and the molasses region). At the end of the loading, the LVIS lasers are switched off using the shutter. The shutter remains closed until the detection of the atoms after their second Ramsey interaction has finished. The fountain total cycle time is T_c=1.145 s. This is 0.25 s shorter than the cycle time used previously but results in a similar atom number [1].

For collisional shift measurements, a molasses loading period of 750 ms is chosen, and the atomic density is changed every 1000 s. During low-density operation, the LVIS lasers are blocked during the first 500 ms of the loading period. Thus, atoms are loaded only during the remaining 250 ms, resulting in the same cloud density as in normal operation.

During the high-density operation, the LVIS lasers are on during the entire loading period. The total cycle time is 1.645 s, and all cycle parameters for operation at low and high atom densities are identical with the exception of the LVIS shutter. The ratio between the measured high and low atom densities is ~10, as compared to a factor of ~2 previously when thermal vapor loading was used. For this reason and because of the reduced contribution from the Dick effect [4], the collisional shift is measured with improved statistical uncertainty. As the collisional shift estimation assumes a proportionality between atomic density and fluorescence signal, we attribute a 10% systematic uncertainty to the collisional shift correction [1]. This uncertainty is added in quadrature to the statistical uncertainty of the collisional shift correction. Typically, the magnitude of the collisional shift correction is on the order of 1×10^{-15}, and the total collisional shift uncertainty contribution to the error budget of the fountain is on the order of 0.25×10^{-15} for two 24-hour measurements (see Table 1). The two measurements are generally performed immediately before and after a fountain evaluation.

PERFORMANCE OF CSF2

For quantum projection noise-limited operation of a fountain, the signal-to-noise ratio is $SNR = (N_{at})^{1/2}$ where N_{at} is the number of detected atoms. Utilizing the slow atom source for loading, quantum projection noise-limited operation of CSF2 was verified experimentally by applying two $\pi/4$-pulses and measuring SNR over a range of values of N_{at} [1]. If microwave oscillator noise does not contribute the according short-term frequency instability $\sigma_y(1s)$ of the fountain is given by [5]:

$$\sigma_y(1s) = \frac{1}{\pi \times Q_{at} \times SNR}\sqrt{T_c / 1s} \qquad (1)$$

where Q_{at} is the atomic line quality factor and T_c is the cycle time in seconds. In Fig. 1 the dashed black line shows the instability $\sigma_y(1s)$ calculated by (1) taking into account the measured SNR for a range of atom loading times which correspond to a range of detected atom numbers. It is thus demonstrated that in CSF2 instabilities $\sigma_y(1s) < 4\times10^{-14}$ can be reached if instability contributions due to local oscillator noise can be neglected.

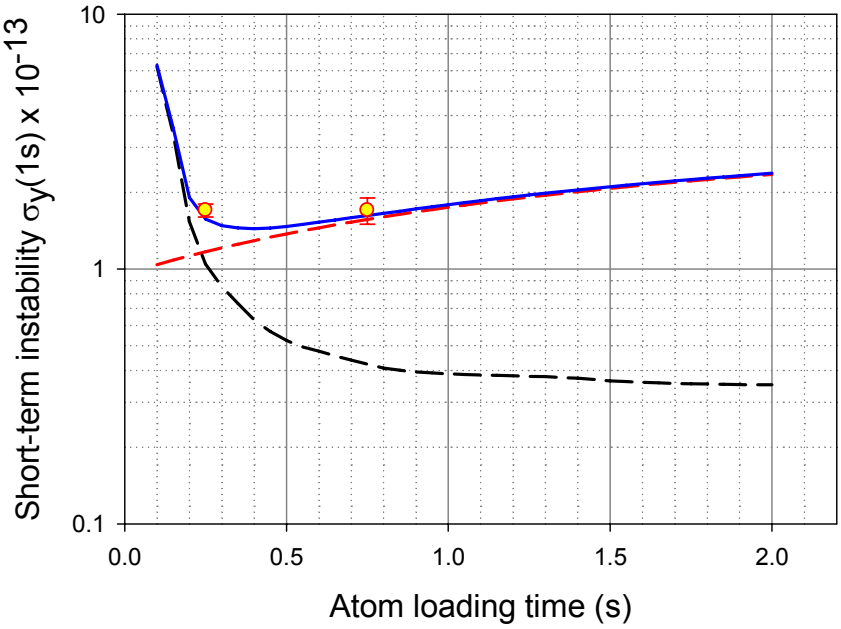

Fig. 1. Allan standard deviation $\sigma_y(1s)$ for different atom loading times. Dashed black line: Calculated $\sigma_y(1s)$ based on measured signal-to-noise ratios SNR (two $\pi/4$-pulses) using (1). Dashed red line: Calculated $\sigma_y(1s)$ due to the Dick effect. Blue line: Both instability contributions added in quadrature. Data points: Frequency instabilities obtained for actual frequency measurements using two different atom loading times.

The contribution of the local oscillator to the short-term fountain instability manifests itself through the Dick effect [5]. It is caused by the presence of a dead time - the local oscillator frequency is measured only between the two Ramsey interactions, and not during the entire cycle time T_c. The corresponding instability contribution for CSF2 has been calculated based on the quartz phase noise data taken from its data sheet and is shown by the dashed red line in Fig. 1. Adding both instability contributions in quadrature yields the blue curve in Fig. 1, which represents the instability expected from the measured *SNR* (two π/4-pulses) and the quartz phase noise data. The two data points in Fig. 1 show actually measured instabilities for normal fountain operation (250 ms loading time) and high density operation (750 ms loading time), which agree well with the calculated blue curve.

As deduced from (1) and demonstrated in Fig. 1, a higher detected atom number reduces the short-term instability of the fountain by improving the signal-to-noise ratio *SNR*. If this is achieved by using longer loading times, it does not automatically lead to a significant reduction of the short-term instability due to the longer cycle time T_c and a correspondingly larger contribution to the instability from the local oscillator noise as the dead time is longer (see Fig. 1). Here the advantage of utilizing a slow atom beam for loading becomes obvious: It reduces the time required to load a specific atom number N_{at}. For the same quantum projection noise determined by N_{at}, the shorter loading time corresponds to a shorter total cycle time T_c and a smaller Dick effect contribution.

The fractional frequency instability (Allan standard deviation) of CSF2, measured against two hydrogen masers, is shown in Fig. 2. The short-term instability of CSF2 is measured to be $\sigma_y(1s)=1.7\times10^{-13}$, with removed noise contribution from the maser. The maser drift starts to limit the long-term instability above several thousand seconds of measurement time.

A plot of recent collisional shift slope measurements is illustrated in Fig. 3. The improvement of the collisional shift slope uncertainty after January 2010 due to the utilization of the LVIS is evident. The reduction of collisional shift slope uncertainties allows us now to better check the assumed proportionality between atomic density and fluorescence signal amplitude by measuring collisional shift slopes for a wide range of atomic densities.

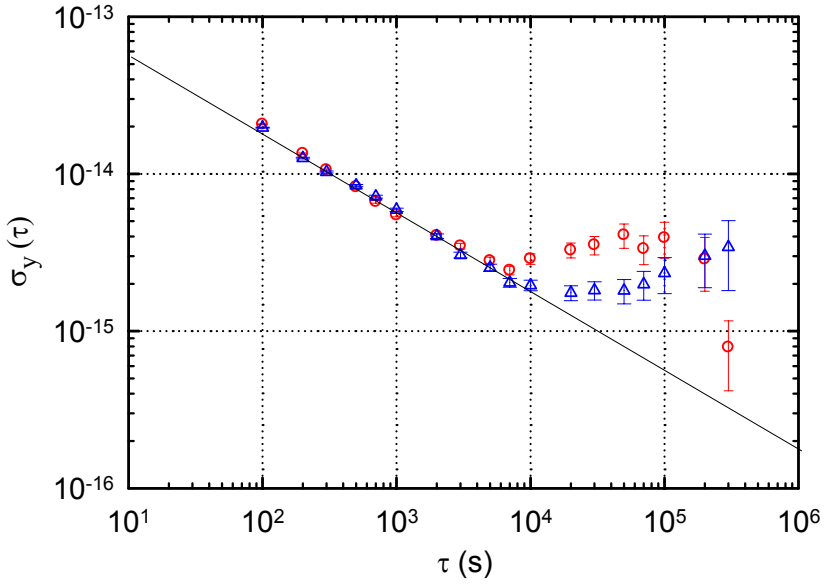

Fig. 2. Fractional frequency instability of CSF2 against the PTB hydrogen masers H5 (red circles) and H6 (blue triangles). The full line represents an instability of $\sigma_y(\tau)=1.7\times10^{-13}\ (\tau/s)^{-1/2}$.

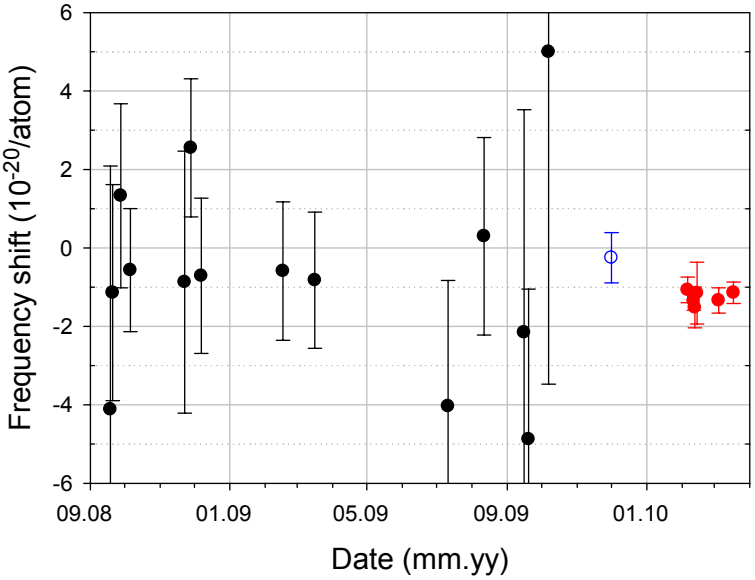

Fig. 3. Collisional shift slopes of CSF2. Solid black triangles represent data taken over several days each with loading from thermal background. The open blue circle indicates the weighted average of this data. Solid red circles represent data taken in a day each using the LVIS (at normal operation with LVIS, 9×10^4 atoms are detected).

MICROWAVE POWER DEPENDENCE

Because of the reduced statistical uncertainty of collisional shift evaluations, the dominant contribution to the CSF2 uncertainty budget is now due to the observed microwave power dependence of the output frequency [1]. A similar, even more pronounced microwave power dependence was previously observed with the PTB-CSF1 fountain [6]. Many efforts have already been made to clarify the origin of the measured frequency shifts in the 10^{-15} range. At this level, frequency shifts due to unaccounted collisional effects, microwave leakage, Majorana transitions, Rabi and Ramsey pulling or spurious microwave components could be excluded for both PTB fountains.

Recently we started to investigate the frequency shifts due to longitudinal phase gradients. These phase gradients are primarily due to the endcap losses in current microwave cavities [7]. The azimuthally symmetric phase variations produce large distributed cavity phase errors for two 2π, 4π, and 6π pulses, because of the correlation between the transverse variation of the Rabi frequency over the cavity aperture with a density variation of the atoms, along with the symmetry of the longitudinal phase variation in the cavity [8].

We calculated the distributed cavity phase errors for the PTB fountain clock CSF1 cavity, using the measured atom cloud sizes on the way up and down. The difference of the cloud sizes on the two cavity traversals gives different average Rabi frequencies to the atoms for the two traversals. This is required for the longitudinal phase gradients to produce a distributed cavity phase error. This same difference is also required for frequency shifts due to microwave leakage fields interacting with the atoms between the two Ramsey interactions [9].

In Fig. 4 we show the resulting calculated changes dP in transition probability for a range of microwave amplitudes together with first experimental results. *b* is a multiplier for the microwave field amplitude that gives the number of $\pi/2$-pulses during a cavity traversal. For normal operation at "optimum" microwave power, *b* is set to be 1. The experimental results were obtained by measuring the frequency difference between the fountains CSF1 and CSF2, with CSF2 constantly operated at $b = 1$ and changing *b* for CSF1. Frequency corrections due to the quadratic Zeeman effect, blackbody radiation, gravity and the relativistic Doppler effect were applied to both fountains. While a constant collisional shift slope could be used for the correction of the collisional frequency shift of CSF2, the proper collisional shift slope for each setting of *b* needed to be determined and applied for CSF1, because the variation of *b* resulted in significantly different clock state compositions after the first Ramsey interaction and thus in different collisional shift slopes [10]. The observed frequency difference between CSF1 and CSF2 when both fountains were operated at

optimum microwave power was $(1.0 \pm 0.4)\times10^{-15}$, which is compatible with the combined systematic uncertainties of both fountains. This frequency offset was subtracted from all the measured frequency differences between CSF1 and CSF2, so that the frequency difference at $b = 1$ for both fountains was arbitrarily set to be zero. The transition probability changes shown in Fig. 4 were calculated from this frequency differences and the Ramsey fringe slopes measured at each b.

The calculated transition probability agrees well with the measurements in Fig. 4. This suggests that the previously reported microwave power dependence of the CSF1 output frequency is explained by longitudinal phase gradients of the microwave field in the Ramsey cavity. The calculations show that these phase gradients produce large frequency shifts at elevated microwave power, whereas the shift at optimum power is well below 10^{-16}. The measurements in CSF1 around $b = 1$ showed deviations from the calculated results, suggesting that another perturbation is present. We are currently investigating these frequency shifts.

A magneto-optical trap was used for the measurements with CSF1 in Fig. 4. In CSF2, the atoms are cooled with optical molasses, resulting in a much larger cloud size and considerably reducing the longitudinal distributed cavity phase errors (Fig. 4, blue curve). Preliminary experimental results confirm this. Further investigations will soon begin to reduce the entry in the uncertainty budget related to microwave power dependence (Table 1).

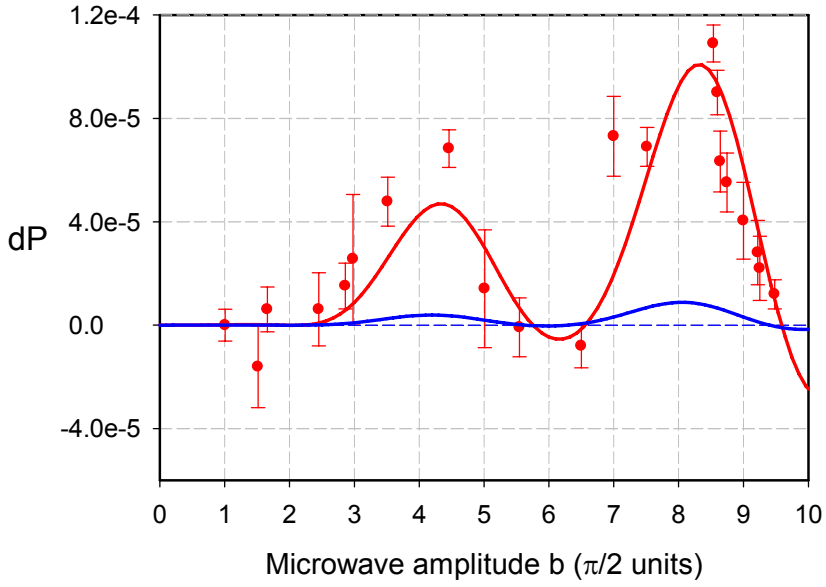

Fig. 4. Calculated and measured transition probability changes due to longitudinal phase gradients for the fountains CSF1 (red curve and data points) and CSF2 (blue curve).

UNCERTAINTY BUDGET

With molasses loading from a thermal caesium vapor, the uncertainty budget of CSF2 was previously dominated by the statistical uncertainty of the collisional shift correction. The new atomic source allows a significant reduction of the total uncertainty of CSF2 to below 0.6×10^{-15}, as shown in Table 1.

Table 1. Budget of systematic uncertainties of CSF2 (in parts in 10^{15}).

FREQUENCY SHIFT	CORRECTION	UNCERTAINTY
Quadratic Zeeman	-99.85	0.06
Blackbody radiation	16.60	0.06
Gravity+Relativistic Doppler	-8.567	0.006
Collisional shift	1.0	**0.25**[(1)]
Transverse cavity phase	0	0.15
AC Stark	0	0.001
Majorana transitions	0	0.0001
Rabi pulling	0	0.0002
Ramsey pulling	0	0.001
Electronics	0	0.2
Microwave leakage	0	0.1
Microwave power dependence	0	**0.4**[(2)]
Background pressure	0	0.05
TOTAL		**0.56**

[(1)]Uncertainty with loading from thermal vapor was 0.6×10^{-15}.
[(2)]Leading term in the new uncertainty budget.

The uncertainty due to the collisional shift can be further reduced after the method of rapid adiabatic passage [11] is implemented as planned. We will next focus on reducing the uncertainties arising due to the observed microwave power dependence and the frequency synthesis and locking.

CONCLUSIONS

A new source of slow atoms was recently installed on the caesium fountain CSF2 at PTB. This source allows the short-term instability $\sigma_y(1s)$ of CSF2 to be reduced from 2.5×10^{-13} to 1.7×10^{-13}. Because of the reduced atom loading time and the higher number of atoms, the collisional shift uncertainty is no longer the largest term in the uncertainty budget. The uncertainty is now dominated by the uncertainty contribution due to the observed microwave power dependence of the output frequency. Measurements with the CSF1 fountain suggest that the longitudinal cavity phase gradients produce the observed frequency shifts at elevated power. For normal operation related shifts in CSF1 are expected to be much less than 1×10^{-16}. Due to the larger cloud size associated with the optical molasses used for cooling in CSF2, the effects of longitudinal phase gradients will be even further suppressed in CSF2.

N. N. acknowledges support by the Deutsche Forschungsgemeinschaft.

REFERENCES

[1] V. Gerginov, N. Nemitz, S. Weyers, R. Schröder, D. Griebsch, R. Wynands, "Uncertainty evaluation of the caesium fountain clock PTB-CSF2," *Metrologia*, vol. 47, pp. 65-79, December 2009.

[2] Z. T. Lu, K. L. Corwin, M. J. Renn, M. H. Anderson, E. A. Cornell, C. E. Wieman, "Low-Velocity Intense Source of Atoms from a Magneto-optical Trap," *Phys. Rev. Lett.*, vol. 77, pp. 3331-3334, June 1996.

[3] N. Nemitz, V. Gerginov, D. Griebsch, R. Wynands, S. Weyers, "Utilization of an atomic Low-Velocity Intense Source (LVIS) in a primary fountain frequency standard," unpublished.

[4] G. J. Dick, "Local oscillator induced instabilites in trapped ion frequency standards", *Proc. 19th Annual Precise Time and Time Interval (PTTI) Applications and Planning Meeting, Redondo Beach, CA*, pp. 133-147 , December 1987.

[5] A. Clairon, P. Laurent, G. Santarelli, S. Ghezali, S. N. Lea, M. Bahoura, "A Cesium Fountain Frequency Standard: Preliminary Results," *IEEE Trans. Instrum. Meas.*, vol. 44, pp. 128-131, April 1995.

[6] S. Weyers, R. Wynands, K. Szymaniec, W. Chalupczak, "Multiple $\pi/2$ Pulse Area Operation of Caesium Fountains and the Collisional Frequency Shift," in: *Proc. 21th European Frequency and Time Forum (EFTF) and 2007 IEEE International Frequency Control Symposium (FCS), Geneva*, pp. 52-54, May 2007.

[7] R. Li, K. Gibble, "Phase variations in microwave cavities for atomic clocks," *Metrologia*, vol. 41, pp. 376-386, October 2004.

[8] R. Li, K. Gibble, "Distributed Cavity Phase and the Associated Power Dependence," in: *Proc. 2005 Joint IEEE International Frequency Control Symposium and Precise Time and Time Intervall (PTTI) Systems and Applications Meeting, Vancouver, BC, Canada*, pp. 99-104, August 2005.

[9] S. Weyers, R. Schröder, R. Wynands, „Effects of microwave leakage in caesium clocks: theoretical nad experimental results", *Proc. 20th European Frequency and Time Forum (EFTF)*, *Braunschweig*, pp.173-180, March 2006.

[10] K. Szymaniec, W. Chalupczak, E. Tiesinga, C. J. Williams, S. Weyers, and R. Wynands, "Cancellation of the Collisional Frequency Shift in Caesium Fountain Clocks," *Phys. Rev. Lett.*, vol. 98, pp. 153002-1, April 2007.

[11] F. Pereira Dos Santos, H. Marion, S. Bize, Y. Sortais, A. Clairon, C. Salomon, "Controlling the Cold Collision Shift in High Precision Atomic Interferometry," *Phys. Rev. Lett.*, vol. 89, pp. 233004-1, December 2002.